Responsive nanozeolites: Smart porosity and surface tailoring for multimodal imaging and therapy of cancer

Kristina Djanashvili, Éva Tóth

LE STUDIUM
Loire Valley
Institute for Advanced Studies

LE STUDIUM Multidisciplinary Journal

www.lestudium-ias.com

FELLOWSHIP FINAL REPORT

Responsive Nanozeolites: Smart Porosity and Surface Tailoring for Multimodal Imaging and Therapy of Cancer

Kristina Djanashvili,[1,2,3], Éva Tóth[3]

[1] Delft University of Technology, Department of Biotechnology, Van der Maasweg 9, 2629HZ Delft, The Netherlands
[2] Le Studium, Loire Valley Institute for Advanced Studies, 1 Rue Dupanloup, 45000 Orléans, France
[3] Centre de Biophysique Moléculaire, CNRS, Rue Charles Sadron, 45071 Orléans Cedex 2, France

REPORT INFO

Fellow: Dr Kristina DJANASHVILI
From Delft University of Technology
Host laboratory in region Centre-Val de Loire: Centre de Biophysique Moléculaire, CNRS
Host scientist: Dr Éva TÓTH
Period of residence in region Centre-Val de Loire: January 2017 – January 2018

Keywords :
Zeolites, Porous Nanoparticles Radiolabeling, MRI Contrast Agents, Relaxivity, Water Exchange, PEGylation

ABSTRACT

Effective cancer treatment requires its early diagnosis in combination with safe drug delivery mechanisms. Up to date many therapeutics have failed due to their limited ability to reach the diseased site selectively without damaging healthy cells. Furthermore, none of the existing imaging techniques is absolutely reliable due to the differences in resolution and sensitivity. Therefore, synergistic combination of imaging modalities in one, typically nanodimensional, probe is the key-strategy to benefit from, for example the sensitive and quantifiable PET signal and the high resolution of MRI. Nanozeolites are among the most promising candidates for realization of this concept due to their unique crystalline structure capable of stable hosting of metal-ions with diagnostic and therapeutic properties. Even though, these materials have found many applications in various technologies, their medicinal potential still requires thorough investigations. This project aimed at the design, preparation and testing of novel nanozeolitic probes that can be
applied as personalized drugs for diagnostic and therapeutic purposes.

1- Introduction

Cancer is the second most frequent non-communicable disease worldwide, with 14 million new cases diagnosed in 2012 and an expected incidence of 21 million in 2030.[1] This has a major impact on the world economy. The desire to cure or to improve the quality of life of patients suffering from this disease is driving the development of advanced diagnostics and curative/palliative therapies. Important factors in this context are the minimal invasiveness and the specificity of the procedures applied. The recent progress in medicinal sciences is to a large extent due to the rapid developments in medical imaging that allows for early detection based on the combined information on anatomy, physi- ology and molecular events in tissues and organs. However, there is no single imaging technique capable to deliver such information in one diagnostic session. Therefore, the main focus in the current research lies in building hybrid scanners, which on their turn require dedicated multimodal imaging agents. An example of such approach is combination of high-resolution techniques such as magnetic resonance (MRI) with high-sensitivity imaging, e.g. positron emission tomography (PET).[2] Thereby, nanomaterials offer the highest chances for success based on their morpho- logical and chemical properties, such as high surface area, possible porosity, and facile surface chemistry. The latter feature enables endowment of imaging agents with specific functional groups for improved specificity to cancer cells or prolonged blood-circulation times. Nanozeolines are particularly interesting in this respect due to their unique crystalline structure and biocompatibility. The well-defined pores and cavities are built up from AlO_4- tetrahedra that provide the framework with a negative charge. The counterbalancing alkali- ions are easily exchangeable with other cations, such as trivalent lanthanides (Ln(III)). This property becomes very useful for MRI applications, when paramagnetic Gd(III) is

considered for loading into the big cavities of nanozeolites.[3] In MRI, the contrast originates from differences in water content in soft tissues and from variations in the longitudinal (T_1) and transverse (T_2) relaxation times of water protons. Contrast agents (CAs) improve the contrast by reducing the relaxation times with the efficacy expressed as relaxivity r_1-relaxation rate enhancement in $s^{-1}mM^{-1}$ of Gd(III)-ion. The clinically used T_1 MRI CAs (bright contrast) are small Gd(III)-complexes with relaxivities limited to ~5 $s^{-1}mM^{-1}$ at 20 MHz, 37 °C. Therefore, a relatively large local concentration (~100 μM of Gd^{3+}) of CA is required to achieve the desired contrast.[4] One of the strategies to overcome this shortcoming is to exploit nanoparticles (NPs) to deliver high-payloads of paramagnetic ions to the site of interest, such as tumors or arterial plaques with a local boost of contrast as a result. Previously, we have demonstrated that nanozeolite LTL can be used to deliver huge amounts of Gd(III)-ions (up to 40,000 per NP of 20×40 nm) loaded in the big cages.[5] Additionally, the NPs were loaded with Eu(III) confining it in small cavities of LTL with restricted access of water molecules and, hence a strong luminescent signal. In the following studies, we have investigated the mechanism governing the exchange process between water molecules directly coordinated to the para-magnetic metal center inside the pores and the bulk water (**Fig. 1**). The unusually high r_1- and r_2-relaxivities were attributed to the pheno- menon of fast prototropic water exchange through the pores of LTL, forming linear channel structure. Furthermore, both types of relaxivities were found to be pH responsive,[6] which enables an interesting application of Gd- loaded LTL for mapping of tumor environment, whose pH value is 0.5-0.6 units lower than that in the healthy tissues. These exceptional MRI properties inspired us for continuation of the research with this unique nanoprobe providing it with a radiolabel for PET imaging and at the same time, modifying the surface to achieve the optimal *in vivo* blood-circulation without compromising the water exchange mechanism. This research, being conducted at CBM/CNRS/ Orléans in collaboration with CIPA benefitted from fully equipped scientific setting, including animal imaging facilities and cyclotron.

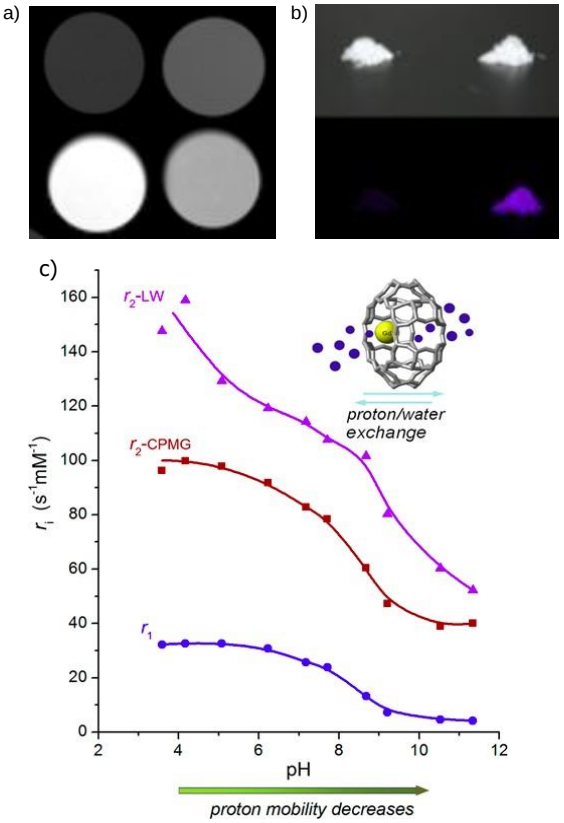

Figure 1. Multifunctional properties of Gd(III)/ Eu(III)-loaded nanozeolite LTL: **a**) MRI images; **b**) luminescence images;[5] **c**) pH response as a result of fast prototropic water exchange mechanism.[6]

2- Experimental details

Synthesis of $mPEG_{2000}$-COOH. $mPEG_{2000}$-OH (5.00 g) was stirred in dry DMF (25 mL) at room temperature until complete dissolution occurred. NaH (461 mg, 60 wt % in oil, 11.52 mmol) was added portion-wise at 0 °C, and the resulting suspension was stirred at 0 °C for 30 min. *t*-Bu-bromoacetate (1.13 mL, 7.68 mmol) was added in once, and the mixture was stirred at RT under inert atmosphere for 18h. MeOH (5 mL) was slowly poured into the reactor and the solvents were removed under reduced pressure. The residue was suspended in H_2O (40 mL) and extracted with DCM (3 × 20 mL). The organic phase was dried over anhydrous Na_2SO_4, filtered and evaporated, and the crude product was purified by column chromatography (SiO_2, DCM/ MeOH 95:5, R_f = 0.2), leading to the desired compound as a yellow wax (4.03 g). This was dissolved in 1:1 TFA/DCM (20 mL), and the mixture was stirred at RT for 2h. After removal of the solvents under vacuum, the

product was obtained as a white solid (3.79 g) and used without further purification. ^{1}H NMR of mPEG$_{2000}$-COOH (400 MHz, 25 °C, D_2O), δ (ppm): 4.15 (s, 2H, C$\underline{H_2}$COO), 3.7-3.5 (m, $CH_2CH_2OCH_3$ + OCH_3CH_2O), 3.47 (*t*, $^3J_{HH}$ = 4.2 Hz, 2H, CH_2OCH_3), 3.38 (s, 3H, CH_3). 13C NMR (100 MHz, 25 °C, D_2O), δ (ppm): 171.5(CO),71−70(OCH_2CH_2O+C$\underline{H_2}CH_2OCH_2$ + C$\underline{H_2}OCH_3$), 69.8 (CH_2COO), 59.0 (CH_3). IR (KBr), cm^{-1}: 3435, 2877, 2537, 1787, 1669, 1454, 1347, 1298, 1167, 950, 848, 811, 781.

Synthesis of mPEG$_{2000}$-Silane. mPEG$_{2000}$-COOH (1.0 g, 0.5 mmol) was mixed with APTMS (174 µL, 1.0 mmol) in DMF (10 mL) in the presence of HBTU (190 mg, 0.5 mmol), HOBt (68 mg, 0.5 mmol) and DIPEA (174 µL, 1 mmol) at RT overnight. After removal of the solvent under reduced pressure, the product was purified by dialysis (MWCO 1 kDa) followed by precipitation in Et_2O, leading to a white solid (875 mg). ^{1}H NMR (400 MHz, 25 °C, D_2O), δ (ppm): 0.59 ($CH_2C\underline{H_2}Si$), 1.56 ($CH_2C\underline{H_2}CH_2Si$), 2.63 ($NC\underline{H_2}CH_2CH_2$), 3.35 ($SiOCH_3$), 3.1-4.5 (mPEG-signals), 8.11 (NH).

Procedures for PEGylation of Gd(III)- Loaded Zeolite LTL. Gd(III)-loaded zeolite LTL (50 mg) was dispersed in a 3:2 mixture of EtOH and water (25 mL), sonicated and vigorously stirred, followed by the addition of 0.5 mL of NH_4OH (25%). To obtain different PEG loading levels, different amounts of a 460 g L^{-1} mPEG$_{2000}$-silane stock solution in water were added to the particle suspension (25 µL for 6.2% PEG-loading). The mixture was gently stirred for 24h and then centrifuged, washed with water (3×) and freeze-dried.

Stability Assessment. The assessment of leaching of Gd(III) ions was performed on zeolite dispersions (1.5 mg mL^{-1}) in water, physiological saline (0.9 w/v%), serum (20 v/v%), and lactate (2.5 mM), respectively. After being incubated in a shaker at 37 °C for 24h, the supernatant was collected and analyzed by the xylenol orange complexation method using UV−vis spectroscopy, as reported previously.[7]

Relaxometric studies and ^{1}H NMRD profiles. The samples were prepared by dispersing 2.5 mg of Gd-LTL or PEGylated Gd-LTL NPs in 1.0 mL of Milli-Q water using a sonication bath and stabilized by adding 1.0g of 1% xanthan gum solution. The pH of the samples was adjusted by addition of either 0.1 M HCl or 0.1 M NaOH. The pH dependence of longitudinal (r_1) and transversal (r_2) relaxivities was investigated on a Varian Inova 300 NMR spectrometer at 25 °C. After careful shimming, the line widths and peak positions were determined by fitting Lorenzian functions to the ^{1}H NMR spectra. Longitudinal relaxation times were measured with the inversion recovery method,[8] whereas transverse relaxation times were measured with the Carr-Purcell-Meiboom-Gill (CPMG) pulse sequence in which the length of the spin echo train was varied[9] with an echo time of 0.5 ms applied. ^{1}H NMRD profiles were acquired on a fast field-cycling Stelar SmartTracer relaxometer with magnetic field varying from 0.00024 to 0.25 T (0.001 to 10 MHz ^{1}H Larmor frequencies). Additional data points in the range of 20-70 MHz were collected on a Bruker WP80 NMR electromagnet, as well as a separate point at 300 MHz on a Varian Inova 300 NMR spectrometer.

MR Imaging. MRI experiments were conducted on a BioSpec 94/21, 9.4 T horizontal magnet (Bruker BioSpin) equipped with BG060 gradient system (950 mT m^{-1} maximal strength and 60 mm inner diameter) and Paravision 5.1 software (Bruker BioSpin). T_1- and T_2-weighted MR images were acquired with spin-echo sequence (RARE sequence with one echo to get a small echo time (TE) and to make the effective-TE equal to TE) at 25 °C. T_1- weighted images were acquired with 29.9 ms TE and varying TR (repetition time) and from 37 to 1500 ms, 137×137 mm^2 resolution with a matrix 256x256 in 16 min acquisition. T_2-weighted images were acquired with varying TE from 19.9 to 79.60 ms, TR of 1000 ms, and 137×137 mm^2 resolution with a matrix 256×256 in 19 min. All images have 1.0 mm slice thickness.

Radiolabeling with ^{89}Zr. Radioactive ^{89}Zr produced by BV cyclotron VU (The Netherlands) was used for the *radiolabling-1* procedure, while for radiolabling-2 production was done at CIPA-cyclotron (France). For the radiolabling-1, 1.0 MBq ^{89}Zr (30 µL in oxalic acid) was added to 1.0 mL of Na-LTL suspension (1.0 mg/mL) followed by incubation at 55 °C for 1.5h, pH 3.5. In *radiolabeling-2* procedure, 5 mg of Na-LTL were suspended in water and 30 mL of $^{89}ZrCl_3$ solution (100 MBq, 6.7×10^{-11} mol ^{89}Zr) were added and the

suspension was stirred for 1.5h at 45 °C. In both procedures after incubation suspensions were centrifuged at 10,000 rpm for 5 min, the radioactivity of both supernatant and precipitate were measured and the labeling yield was calculated. An additional step in radiolabeling-2 procedure included PEGylation of the surface for which a solution of PEG-silane (45 mg in 0.1 mL of water) was added to 5 mg of Zr-LTL re-suspended in 2.5 mL of EtOH(1) : water(1) and 50 mL of NH_4OH (25%). The resulting suspension was stirred for 24h at RT, centrifuged-washed-centrifuged, and re- suspended in 1 mL PBS for the injection of 0.15 mL, 10 MBq.

PET/CT phantoms and radioactivity measurements. Images were acquired with a NanoPET-CT TM preclinical animal scanner (Mediso Ltd., Bioscan Inc.). The image acquisition was set in list mode format.[10] Acquisition time was 15 min. OSEM was used as the reconstruction method (6 subset s, 8 iterations, 0.29 mm pixel size, and 0.585 mm axial thickness) based on SSRB 2D LOR re-binning (linear interpolation, 16 span-size). The CT images were acquired with 55 kVp tube voltage, 1.2 s exposure time in 360 projections. The images of PET/CT modalities were fused using InVivoScope (Bioscan) software. The radioactivity of the obtained samples was measured with a dose calibrator (CRC-25R, Carpintec, USA) or a gamma-counter (1282 CompuGamma, LKB Wallac, Finland).

Animals. Healthy nude mice (3×. ~20 g) were used for MRI experiments and treated in accordance with animal welfare polices of French Ministry of Agriculture. After application of anesthesia (1.5% isoflurane and O_2/N_2O (1:1), 0.7 L/min), mice were injected with 100 µL of LTL-PEG (6 wt%) suspension (pH 7.4) loaded either with Gd(III) or ^{89}Zr.

Imaging experiments. After injection with the Gd-loaded probe, animals were positioned in a custom-built cradle. Respiration was monitored during the whole experiment using an air pillow and body temperature was maintained constant at 37 ºC by a warm-water circulation system. MR acquisitions were performed on a 9.4T horizontal ultrashielded superconducting magnet dedicated to small animal imaging (94/20 USR Bruker Biospec, Wissembourg, France) and equipped with a 950mT/m gradient set. A Bruker 35 mm inner diameter birdcage coil was used for both ^1H transmission and reception. Both coronal and axial images of the brain were obtained using a spin echo RARE sequence with the following parameters: TE/TR 46 ms/5 s, FOV size 1.7×1.7 cm, matrix size 128×128, Bandwidth 50 kHz, slice thickness 1 mm to display (133×133) μm^2 in plane resolution for a duration of 2 min (2 accumulations). Imaging of animals injected with ^{89}Zr-LTL were done with NanoPet/CT Bioscan.

3- Results and discussion

The surface of cylindrical NPs of zeolite LTL with the dimensions of 20 × 40 nm loaded with Gd(III)-ions[5] was conjugated with methoxy-polyethylene glycol ($mPEG_{2000}$). For the covalent attachment of PEG chains to the surface of LTL, the trimethoxysilane derivative of mPEG was prepared by conversion of $mPEG_{2000}$-OH to $mPEG_{2000}$-COOH, followed by the reaction with (3-aminopropyl)-trimethoxy- silane (APTMS) to form the corresponding amide. Full characterization of the PEG- derivatives was done by Fourier transform infrared (FT-IR), nuclear magnetic resonance (NMR) spectroscopies, and atomic force microscopy (AFM), confirming PEGylation and revealing grafting regimes is described in the corresponding publication.[11]

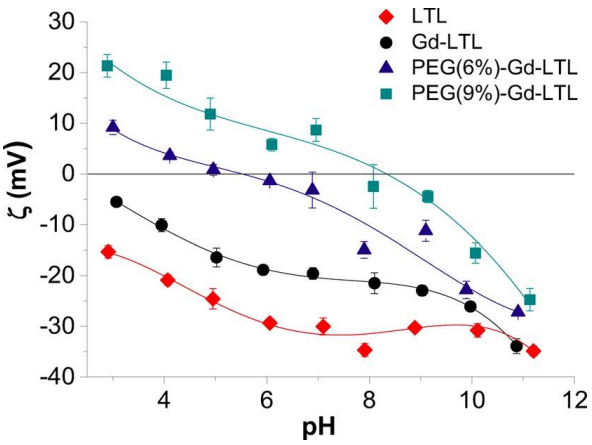

Figure 2. Zeta potential (ζ) as a function of pH: non-PEGylated LTL with 0 and 5.2 wt % Gd; PEGylated Gd-LTL (5.2 wt % Gd) with 6.2 wt % PEG and 9.1 wt % PEG. The curves are guides to the eye.

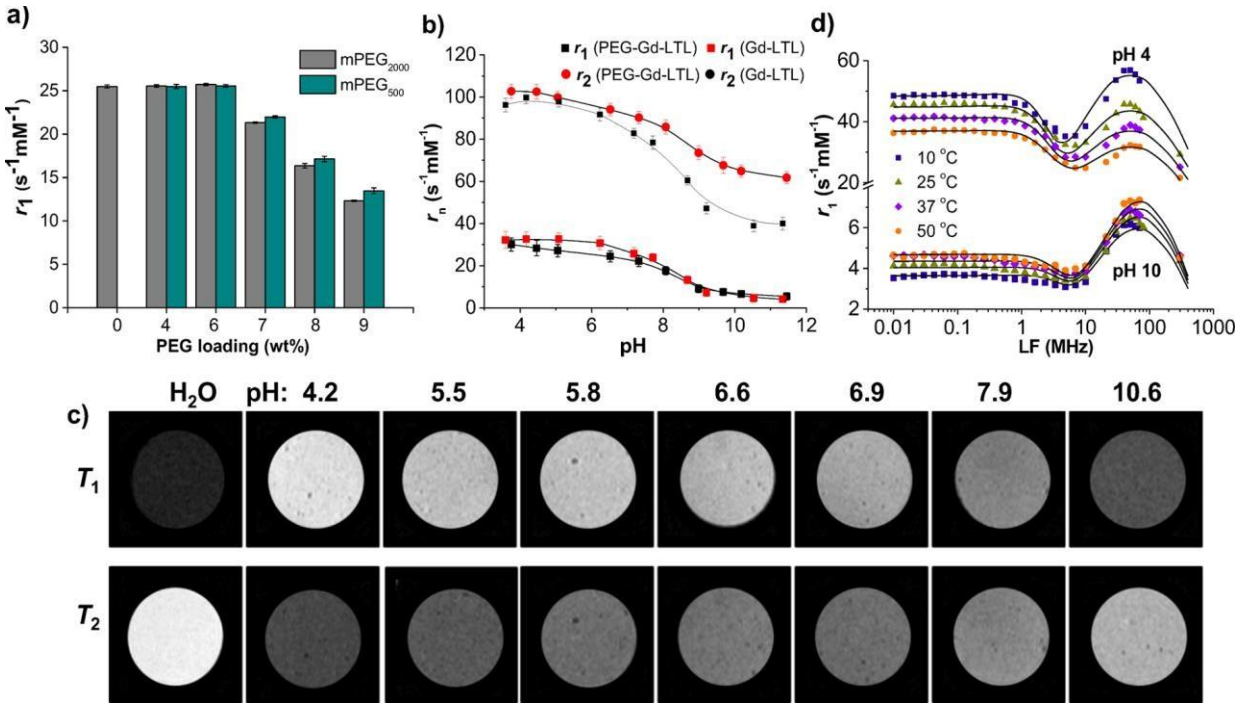

Figure 3. Relaxometric studies on aqueous suspension of Gd-loaded LTL (5.2 wt% Gd) stabilized with 0.5% xanthan solution, 300 MHz, 25 °C: **a**) r_1 of Gd-LTL (pH 5.5) vs increasing loading of PEG_{2000} and PEG_{500}; **b**) r_1 and r_2 of non-PEGylated and PEGylated (6.2 wt% PEG_{2000}) Gd-LTL as a function of pH (the curves are guides to the eye); **c**) MR phantoms of PEGylated (6.2 wt% PEG_{2000}) Gd-LTL (0.3 mM of Gd) as a function of pH (9.4T, 25 °C), top: T_1-weighted spin−echo images, TE = 29.9 ms; bottom: T_2-weighted images, TR = 1 s; **d**) ^{1}H NMRD profiles of PEGylated Gd-LTL (6.2 wt % PEG) at pH 4 and pH 10 and 10, 25, 37, and 50 °C.[11]

Observation of pH-dependency by zeta-potentials confirms PEGylation (**Fig. 2**). Intrinsically, LTL nanocrystals possess a negative zeta potential (ζ = − 32.2 mV), which slightly increases after ion-exchange with GdIII (ζ = − 23.8 mV, 5.2 wt% Gd-loading). PEGylation further reduces the overall charge (ζ = −16.9 mV (6.2 wt % PEG) and −3.3 mV (9.1 wt% PEG)) due to the charge shielding effect. On the one hand, native and Gd-loaded LTL samples show negative ζ in the whole pH range studied without an isoelectric point (IEP). The negative charge increasing with pH (−35 mV at pH 11) is related to the deprotonation of Si-OH groups; similar results have been observed for silanol-rich mesoporous silica NPs.

For PEGylated Gd-LTL, the ζ-values turn from positive to negative between pH 3 and 11 with an IEP at pH 5.6 and 8.3 for 6.2 and 9.1 wt% of PEG-loading, respectively. The changeover, becoming more pronounced with increasing PEG-grafting, is in good agreement with the results by He et al.,[12] who demonstrated that mesoporous silica NPs become less negatively charged upon increase of PEG-loading. Interestingly, the ζ-values of both PEGylated samples reach −27 mV at pH 11, which is only slightly above the ζ-value of the non-PEGylated samples. This similarity with the non-PEGylated samples can be attributed to deprotonation of the surface Si−OH groups that remained unsubstituted by mPEG-silane as the PEG alone is not expected to contribute to the negative charge at pH 11. Consequently, the observed IEP of the PEGylated Gd-LTL samples strongly depends on degree of PEGylation, and results from an interplay between protonation of the PEG ether oxygens and deprotonation of the silanol groups. The changeover from the mushroom to the brush PEGylation regime nicely studied by AFM can directly be related to the r_1 relaxivity values for aqueous suspensions of Gd-LTL with a PEG-content varying from 0 to 9.1wt % (**Fig. 3a**). Although relaxivity remains constant (≈ 25 s^{-1} mM^{-1}) and identical to that of the non- PEGylated LTL up to 6.2 wt% PEG_{2000}, it decreases considerably at higher PEG content and drops to 12.3 $s^{-1}mM^{-1}$ at 9.1 wt% PEG

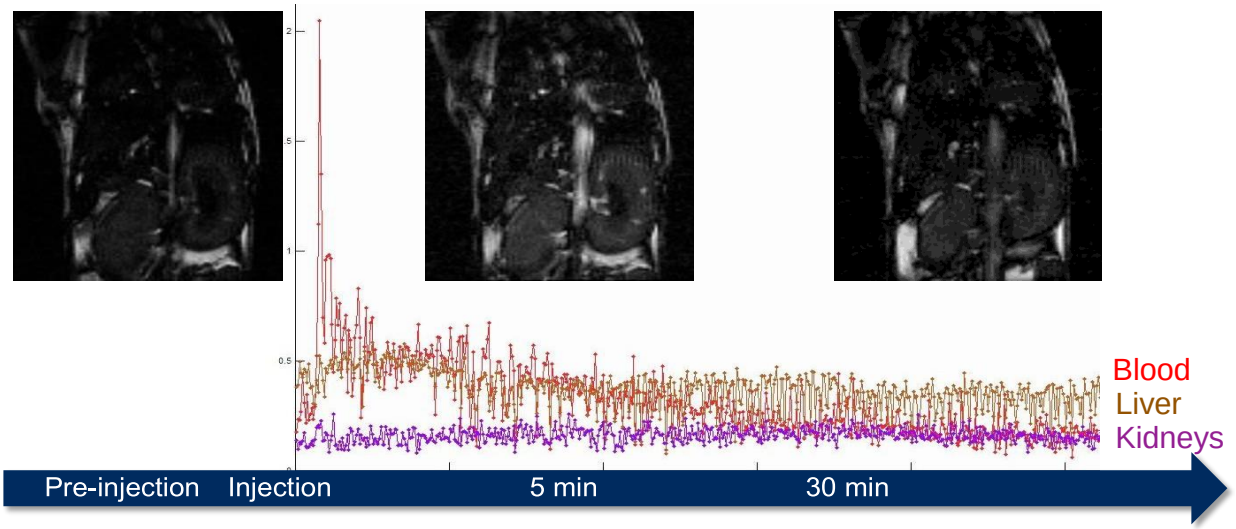

Figure 4. Kinetic MRI study after injection of 100 µL of Gd-LTL-PEG (6 wt%) in PBS buffer, with the Gd-concentration of 0.07 mmol kg^{-1}. The images were taken prior to injection, immediately after (5 min) and after 30 min. The curves represent decrease of relaxivity a after initial peaking in the heart immediately after injection.

(maximum degree of PEGylation that could be reached for this zeolite). Similar behavior was observed for the Gd-LTL functionalized with shorter PEG_{500} chains, indicating no effect of the length of PEG-chains (**Fig. 3a**). The PEG brushes compactly arranged at the surface increasingly slow down water exchange and limit water access to Gd(III), which explains the decline in relaxivity above 6.2 wt% PEG. Below this PEG-density, neither r_1/r_2 relaxivities nor the relaxometric pH-response are affected (**Fig. 3b**). Our previous investigations on the rela- xation mechanism revealed that above pH 7 the water structuring inside the zeolite is disrupted by ionization of the silanol groups, Gd(III)- bound water molecules, and decreased con- centration of hydronium ions.[6] This effect is less pronounced in case of the PEGylated Gd- LTL, resulting in a slightly less decrease of r_2 (Δr_2 = 22 $s^{-1}mM^{-1}$) compared to that of the non- PEGylated analogue (**Fig. 3b**).

The T_1- and T_2-weighted MR images of PEG- Gd-LTL phantoms (**Fig. 3c**) at pHs ranging from 4.2 to 10.6 are in accordance with the pH-relaxivity curves showing respective decrease and increase of the signal intensity. Nuclear magnetic relaxation dispersion (NMRD) profiles acquired on aqueous suspensions of Gd-LTL and PEG-Gd-LTL (6.2 wt% PEG) at pH 4 and 10 to assess the rotational dynamics of the system are similar for both PEGylated and non-PEGylated systems (**Fig. 3d**). Detailed analysis of the NMRD profiles reported in the paper confirms the assumption that the water exchange rate dramatically decreases by the pH increase from 4 to 10 leading to the large relaxivity drop, not effected by PEGylation up to 6 wt%.

T_1-weighted MR imaging was performed on the mice injected with Gd-LTL-PEG. Kinetic study revealed a strong contrast enhancement in the heard and a rapid decrease of relaxivity in time. Interestingly, no accumulation in liver, spleen or kidneys was observed. Analysis of digested organs by ICP did not confirm the presence of Gd(III). This somewhat unexpected result was further evaluated by the PET imaging with the same probe, this time labeled with ^{89}Zr.

^{89}Zr is an upcoming isotope that is not yet widely used in PET imaging, but has good perspectives due to its longer half-life time of 78.4h and decay of β^+ (22.7 %, 0.897 MeV), and electron capture (77 %, 0.909 MeV). Up to now, its application is mainly focused on immuno- PET with ^{89}Zr-labeled proteins and antibo- dies.[13] Therefore, a straightforward method for radiolabeling would make its use in clinics even more attractive. In this study, the initial labeling with ^{89}Zr was performed at pH 3 by incubation of Gd-LTL for 1.5h in the presence of ^{89}Zr in oxalic acid. After purification average radio- labeling yield of 74 ± 5.2 % could be achieved (**Fig. 5a**). ^{89}Zr produced in oxalic acid exists as ^{89}Zr oxalate $[Zr(C_2O_4)_4]^{4-}$, with Zr-coordination number of 8 (Scheme 1).

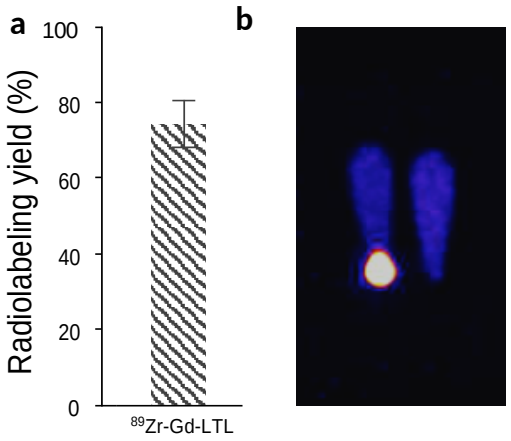

Figure 5. Radiolabeling of Gd-LTL: **a**) the average activity measured by gamma counting after loading with ^{89}Zr-89; **b**) PET phantom image of ^{89}Zr labeled LTL: the centrifuged sample is on the left while the non-centrifuged is on the right.

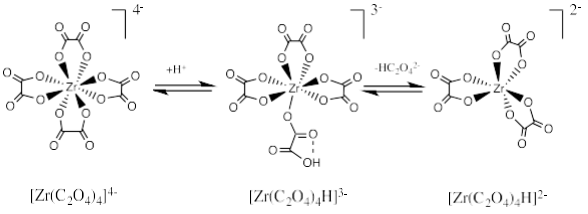

Scheme 1. Formation of Zr-oxalate complexes.

Under acidic conditions the oxalate dissociates to give 6-coordinated $[Zr(C_2O_4)_3]^{2-}$, which creates space on Zr^{IV} for its coordination with silanol oxygen atoms at the surface of LTL.[14] As the calculated diagonal dimension of $[Zr(C_2O_4)_3]^{2-}$ of 7.3 Å is larger than the pore opening of LTL (7.1 Å), it can be assumed that ^{89}Zr coordinates strongly to the oxygens at the surface of LTL rather than to those of the interior. Furthermore, the negative charge of Zr^{IV} complexes present in solution prevents them from entering the negatively charged framework of zeolite LTL. Therefore, it may be concluded that the ^{89}Zr-label is located mainly at the surface of the LTL NPs. The PET phantoms demonstrate the successful radio-labeling of LTL with ^{89}Zr (**Fig. 5b**). The background in images of both centrifuged and non-centrifuged samples appear similar because of the necessary software manipulation during image construction due to the low activity used. Despite good stability of the Zr-89 labeling of the LTL, the loading into the inner cavities is preferred.

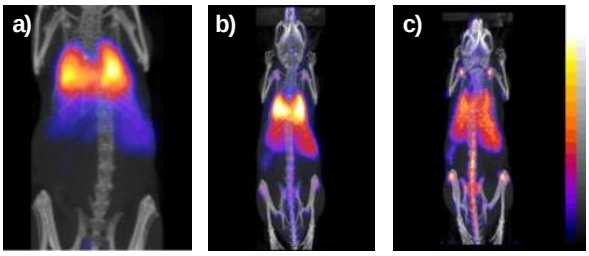

Figure 6. PET imaging after injection of ^{89}Zr-LTL-PEG into mice. Images were taken after **a**) 10 min, **b**) 18h, and **c**) 4d.

Therefore, the radiolabeling-2 procedure was applied in which the radiolabel was used as a chloride salt, followed by PEGylation of the surface. The radiolabeling resulted in a good yield (86%) and the probe was used for the PET imaging.

For the PET imaging, 5 mg of the prepared ^{89}Zr--LTL-PEG probe were diluted in 1 mL of PBS from which 150 µL (10 MBq) were injected into each animal. Images were taken soon after injection (10 min) followed by 18h and the last image after 4d. The images clearly indicate very strong accumulation of the probe in the lungs immediately after administration. In the course of time, a certain amount of ^{89}Zr can be seen spreading out to the liver. The residual amount of ^{89}Zr found in lungs after 4 days was determined to be 6%. Furthermore, it can be assumed that the probe was not disassembled, since the images of the animals injected with free ^{89}Zr showed accumulation in bones exclusively.[15]

These results explain the fact that the probe could not be observed by MRI since the lungs could not be visualized properly with this technique. Obviously, the following studies should be dedication to investigation of the mechanism of the lung accumulation and their unusual subsequent wash-out.

4- Conclusion

In conclusion, we addressed the impact of progressive surface PEGylation of Gd-LTL NPs on their relaxation efficiency, stability and cell toxicity. The existence of two different morphological regimes that PEG, depending on its density, can adopt on the surface of LTL particles was shown to have a significant effect on r_1 relaxivities. We evidenced that although in

the mushroom PEG regime (up to 6 wt%) the particles retain their remarkable pH-responsive relaxivity, at higher PEG density, the more compact PEG layer (brush regime) seriously limits diffusion and exchange of protons/water between the interior of LTL and the bulk. This is important guidance for surface engineering of porous NPs as potential MRI CAs in general, because their relaxation efficiency is closely related to fast exchange between bulk water and water molecules coordinated to Gd(III) in the inner cavities. Ln-loaded LTL has already shown potential for dual T_1–T_2 MRI and optical imaging.[5-6] We demonstrated the benefits of PEGylation and provide general insight into the understanding of how surface functionalization of porous nanomaterials affects fundamental properties like proton exchange as well as more applied features like MRI efficiency. We believe that this work will steer Ln(III)-loaded zeolite LTL particles towards bioapplications.

In vivo MRI revealed interesting behavior of the probe upon its injection into mice. The unexpected disappearance of the probe had found the explanation in PET imaging experiments, revealing accumulation of ^{89}Zr-89 labeled LTL in the lungs. Even though, this behavior could be expected from a nanoprobe such as LTL, its subsequent wash-out to the liver is an interesting finding that deserves a closer look. To have a better understanding of the accumulation, the lungs were extracted, stained with a fluorescent dye and subjected to micro- scopic analysis. This study is still in progress and will hopefully shed light to this question.

Altogether, we have demonstrated novel application of nanozeolites based on their immense structure diversity. Development of facile functionalization methods will increase the attractiveness of these unique probes for multimodal applications in medicine. The pitfalls detected in the course of this research open new avenues for more studies, which will definitely result in new elegant solutions bringing these probes closer to application.

5- Perspectives of future collaborations with the host laboratory

The research groups of Dr. Kristina Djanashvili and Dr. Éva Tóth have a long-standing scientific relationship. Making part of several successive COST Actions working on development of contrast agents for medical imaging, they have already been collaborating on many projects. These interactions were always fruitful, resulting in common scientific papers, many of them as a result of short-term scientific missions accomplished by PhD students and postdocs visiting the labs either in Delft or in Orléans. The research conducted in the framework of Le Studium fellowship was very valuable for gaining new insights in the field of medical imaging after having the opportunity to work in the highly equipped laboratory such as CBM. As mentioned in the conclusion, the research conducted during the fellowship had awoken many exciting and important scientific questions that require more experimental work and creative thinking, which will be done together with the host institute.

At the moment, several publications together with the host institute are already in the pipeline and one book chapter is under the review. Furthermore, both groups are always open for side-projects that come along in science, which can be seen from the publication list going beyond the project.

The network built up during this year at CNRS opened possibilities for new interesting collaborations that were even not envisioned when proposing this research. Currently, there are intensive interactions with dr. Mathieu Allix at CEMTI/CNRS (Conditions Extrêmes et Matériaux: Haute Température et Irradiation). The expertise of his group on porous nanomaterials can be considered as a valuable asset to this research and will possibly result in common proposals for the future research. Last but not least, there is an ongoing collaboration with dr. Chantal Pichon (CBM) on setting up a Erasmus Mundus joint Master Degrees program on *European Master in Applied Biotechnology and Biophysics* together with Universities of Orléans, Zagreb and Krakow. The initial proposal has received very positive evaluation, and despite not being granted in the first attempt, the constructive comments of the reviewers will be considered in the resubmission, which is currently under preparation and will happen soon.

6- Articles published in the framework of the fellowship

The scientific output of the project is represented by published articles and given oral/posters

presentations listed below. Some of the articles belong to the side-projects accomplished in collaboration with the host institute.

Publications

W. Zhang, J. Martinelli, J.A. Peters, J.M.A. van Hengst, H. Bouwmeester, E. Kramer, C.S. Bonnet, F. Szeremeta, É. Tóth, K. Djanashvili. Surface PEG Grafting Density Determines Magnetic Relaxation Properties of Gd-Loaded Porous Nanoparticles for MR Imaging Applications. *Appl. Mater. Interfaces*, **2017**, *9*, 23458−23465.

F. Mayer, S.Tiruvadi Krishnan, D.T. Schühle, S.V. Eliseeva, S. Petoud, É. Tóth, K. Djanashvili, Luminescence Properties of Self-Aggregating Tb^{III}DOTA Functionalized Calix[4]arenes. *Frontiers in Chemistry*, **2018**, *6*, 1-9.

F. Cucinotta, B.P. Jarman, C. Caplan, S.J. Cooper, H.J. Riggs, J. Martinelli, K. Djanashvili, E. La Mazza, F. Puntoriero. Light-Harvesting Antennae using the Host-Guest Chemistry of Mesoporous Organosilica. *ChemPhotoChem*. **2018**, *2*, 196-206.

C. Tsoukalas, S. Geninatti-Crich, A. Gaitanis, T. Tsotakos, M. Paravatou-Petsotas, S. Aime, R. Jiménez-Juárez, C.D. Anagnostopoulos, K. Djanashvili, P. Bouziotis. Tumor targeting via sialic acid: ^{68}Ga-dota-en-pba as a new tool for molecular imaging of cancer with PET. *Mol. Imaging and Biology*, **2018,** *20*, 798-807.

Oral communications:

Towards Multimodal Imaging with Porous Nanodevices. Le Studium Conference – Is Multimodal Imaging an Invention with a Future? The Input of Chemistry. 11-13 December, **2017**, Orléans, France.

Responsive Nanozeolites Smart Porosity and Surface Tailoring for Multimodal Imaging and Therapy of Cancer. Seminar at Centre Biophysique Moléculaire (CBM-CNRS), Orléans, France, 20 January, **2017**.

Challenges and Potential of Chemistry in Design of Theranostic Probes. Le Studium Thursday Seminar Series, 9 May, **2017**, Orléans, France.

Responsive Nanozeolites Smart Porosity asd Surface Tailoring for Multimodal Imaging and Therapy of Cancer. 17 February, **2017**, Conditions Extrêmes et Matériaux: Haute Température et Irradiation (CEMTHI-CNRS), Orléans, France.

Porous Nanostructures as Versatile Stable Chelates for Complexation of Lanthanides for pH Responsive MR Imaging. International Symposium on Metal Complexes, ISMEC 2017, 11-15 June **2017**, Dijon, France.

Advances of Porous Nanomaterials Designed for Multimodal Imaging and Therapy. Annual Meeting of the Dutch Society for Matrix Biology (NVMB), 11-12 May **2017**, Lunteren, The Netherlands.

Posters:

Affinity Study on Gd-DTPA-PEG-Folate to Cervix Cancer Cells Overexpressing Folic Acid Receptors". R. Putri Fauzia, R. Ukun, M.S. Soedjanaatmadja, A. Hardi Gunawan, K. Djanashvili. Le Studium Conference – Is Multimodal Imaging an Invention with a Future? The Input of Chemistry. 11-13 December, **2017**, Orléans, France.

7- Acknowledgements

This work was supported by the Le Studium, Loire Valley Institute for Advanced Studies, Orleans & Tours, France under Marie Sklodowska-Curie grand agreement no. 665790, European Commission.

KD grateful to the host scientist Éva Tóth and her co-workers Célia Bonnet ad Sara Lacerda for the work on the project. Frédéric Szeremeta, Sandra and William Même, (Centre de Biophysique Moléculaire) as well as Isidro Da Silva, Stéphanie Retif and Julien Sobilo (Centre d'Imagerie du Petit Animal) are acknowledged for their support in animal imaging experiments and radiolabeling. Le Studium team is greatly acknowledged for creating a very pleasant scientific and social environment for the fellows and unconditional support and help with all kinds of issues that a foreigner might come across during the stay abroad.

8- References

[1] *Cancer Research UK*, https://www.cancerresearchuk.org, **2018**.
\
[2] H. F. Wehrl, S. Wiehr, M. R. Divine, S. Gatidis, G. T. Gullberg, F. C. Maier, A. M. Rolle, J. Schwenck, W. M. Thaiss and B. J. Pichler, *J. Nuc. Med.*, **2014**, *55*, 11S-18S.

[3] J. A. Peters and K. Djanashvili, *Eur. J. Inorg. Chem.* **2012**, 1961-1974.

[4] S. Aime, M. Botta, M. Fasano and E. Terreno, *Chem. Soc. Rev.* **1998**, *27*, 19-29.
[5] F. Mayer, W. Zhang, T. Brichart, O. Tillement, C. S. Bonnet, E. Toth, J. A. Peters and K. Djanashvili, *Chem.- Eur. J.* **2014**, *20*, 3358-3364.

[6] W. Zhang, J. A. Peters, F. Mayer, L. Helm and K. Djanashvili, *J. Phys. Chem. C* **2015**, *119*, 5080-5089.

[7] A. Barge, G. Cravotto, E. Gianolio and F. Fedeli, *Contrast Media & Molecular Imaging* **2006**, *1*, 184-188.

[8] R. L. Vold, J. S. Waugh, M. P. Klein and D. E. Phelps, *J. Chem. Phys.* **1968**, *48*, 3831-3832.

[9] S. Meiboom and D. Gill, *Rev. Sci. Instrum.* **1958**, *29*, 688-691.

[10] M. d. R. R. Torres, R. Tavare, R. L. Paul, M. Jauregui-Osoro, A. Protti, A. Glaria, G. Varma, I. Szanda and P. J. Blower, *Angew. Chem. Int. Ed. Engl.* **2011**, *50*, 5509-5513.

[11] W. Zhang, J. Martinelli, J. A. Peters, J. M. A. van Hengst, H. Bouwmeester, E. Kramer, C. S. Bonnet, F. Szeremeta, É. Tóth and K. Djanashvili, *ACS Appl. Mat. Interf.*, **2017**, *9*, 23458-23465.

[12] Q. He, J. Zhang, J. Shi, Z. Zhu, L. Zhang, W. Bu, L. Guo and Y. Chen, *Biomaterials* **2010**, *31*, 1085-1092.

[13] a) L. Perk, O. Visser, M. Stigter-van Walsum, M. W. D. Vosjan, G. M. Visser, J. Zijlstra, P. Huijgens and G. M. S. van Dongen, *Eur. J. Nucl. Med. Mol. Imag.* **2006**, *33*, 1337-1345; b) P. K. E. Börjesson, Y. W. S. Jauw, R. Boellaard, R. de Bree, E. F. I. Comans, J. C. Roos, J. A. Castelijns, M. J. W. D. Vosjan, J. A. Kummer, C. R. Leemans, A. A. Lammertsma and G. A. M. S. van Dongen, *Clin. Cancer. Res.* **2006**, *12*, 2133-2140.

[14] J. P. Holland and N. Vasdev, *Dalton Transactions* **2014**, *43*, 9872-9884.
[15] D. S. Abou, T. Ku and P. M. Smith-Jones, *Nucl. Med. Biol.*, **2011**, *38*, 675-681.